Investigation of Rotor Loads and Vibration at Transition Speed

Hyeonsoo Yeo
hsyeo@mail.arc.nasa.gov
Raytheon ITSS
NASA Ames Research Center
Moffett Field, California

Patrick M. Shinoda
pshinoda@mail.arc.nasa.gov
Army/NASA Rotorcraft Division
Aeroflightdynamics Directorate (AMRDEC)
Ames Research Center
Moffett Field, California

Abstract

Blade section normal force and flap bending moment were investigated for UH-60 Black Hawk helicopter rotor operating at transition speed. The measured data from both flight and full-scale wind tunnel tests are compared with calculations obtained using the comprehensive rotorcraft analysis CAMRAD II. There is good agreement for the oscillatory flap bending moments between the flight and wind tunnel tests when the rotor in the wind tunnel was trimmed to match thrust and pitch and roll moments measured on the main rotor shaft in the flight test. The calculations were made using three free wake models: rolled-up, multiple-trailer, and multiple-trailer with consolidation wake models. Both multiple-trailer and multiple-trailer with consolidation models improve the normal force correlation qualitatively, and the magnitude of 1/rev and 2/rev harmonics of flap bending moments. However, none of these wake models appear to be adequate for the accurate prediction of rotor-induced vibration.

Notation

C_p	power coefficient
C_T	rotor thrust coefficient
C_w	weight coefficient
G	strength of trailed vorticity
r	blade radial station
r_C	centroid of vorticity
r_G	moment (radius of gyration) of vorticity
R	bade radius
γ	flight path angle
Γ	bound circulation
μ	advance ratio
σ	solidity

Introduction

The accurate prediction of rotor loads and vibration remains a difficult problem for helicopter design. Typically, helicopters encounter the highest vibration in two different speed regimes, either in a low-speed transition regime or at high speed. Depending upon the helicopter, the transition vibratory loading may be more or less severe than the vibratory loading that builds up at high speed.

Performance and dynamic data are available from flight test for the standard UH-60 blades on a UH-60A airframe [1]. The same full-scale blade has been recently tested in the 80- by 120-Foot Wind Tunnel at Ames Research Center on the Large Rotor Test Apparatus (LRTA) [2]. One of the primary objectives of the wind tunnel test was to measure the rotor performance and loads at low speed for direct comparison with the UH-60A flight test. These extensive test data sets provide a useful resource that can be used to examine loads and vibration in the transition regime.

The importance of the free wake for the prediction of vibratory loads in low speed flight has been demonstrated in Ref. 3. The study showed that the interaction of the blade with tip vortices is fundamental to an accurate prediction of vibratory loads. Recently, new wake models have been developed for tiltrotor analysis and performance and airloads calculations were compared with data from testing of the Tilt Rotor Aeroacoustic Model (TRAM) [4, 5]. By using a free wake geometry

Presented at the American Helicopter Society 58th Annual Forum, Montreal, Canada. June 11-13, 2002. *Copyright © 2002 by the American Helicopter Society International, Inc. All rights reserved.*

calculation method that combines the multiple-trailer wake with a simulation of the tip vortex formation process (consolidation), good correlation was obtained for both performance and airloads. Although a tiltrotor blade is different from a typical helicopter blade, in that the blade has larger twist and loading is concentrated more on the inboard portion of a blade, it is considered to be important to investigate the effect of these new wake models on the vibratory loads of the UH-60A helicopter.

In this study, loads calculations were carried out using the analysis CAMRAD II and the results are compared with the UH-60 flight and wind tunnel test data. The purpose of this study is twofold: 1) understand the similarities and differences in rotor loads and vibration between the flight and wind tunnel tests of the UH-60A rotor in the transition regime where vibration is a concern, and 2) carry out comprehensive calculations using CAMRAD II with various wake models and compare the results with the test data.

Flight and Wind Tunnel Test Data

Flight test data with the UH-60A blades were obtained in the NASA/Army UH-60A Airloads Program conducted from August 1993 to February 1994 [1]. The data used in this study are steady level flight conditions at C_w/σ = 0.08. Those are Flight 85, Counters 8512, 8513, 8514, and 8515, which correspond to the advance ratios of 0.178, 0.149, 0.129, and 0.11 respectively (Table 1).

Wind tunnel test data with the full-scale UH-60A blades were obtained from the NASA Ames 80- by 120-Foot Wind Tunnel test which was conducted in the summer of 2001 [2]. The test data were acquired over a wide range of thrust, speed, and shaft angle including speed sweeps at specific thrusts and rotor shaft angles of attack, and thrust sweeps at specific tunnel velocities and rotor shaft angles of attack. Some test conditions were obtained with the rotor trimmed to match thrust and pitch and roll moments measured on the main rotor shaft in the flight test. These cases are wind tunnel test Run 178, Points 10, 16, 20, and 26, which correspond to the advance ratios of 0.178, 0.149, 0.129, and 0.11 respectively (Table 1). The blade was instrumented with nine bending moment gages. There were 12 pressure transducers located at the leading edge of the blade from 74% R to 96%R. However, those were not enough for the calculation of airloads.

Table 1 Flight and Wind Tunnel Test Conditions

C_T/σ	μ	Airloads Program Flight/Counter	Wind Tunnel
0.08	0.110	8515	Run 178, Pt. 26
0.08	0.129	8514	Run 178, Pt. 20
0.08	0.149	8513	Run 178, Pt. 16
0.08	0.178	8512	Run 178, Pt. 10

Figure 1 shows the measured pitch and roll moments and shaft angle from both the flight and wind tunnel tests. The shaft bending moments from the flight test represent 19 revolutions and the wind tunnel test results are the average of 32 revolutions of data. For wind tunnel operation, the thrust and the rotor pitch and roll moments were trimmed to the flight test measurements for a given shaft angle. The LRTA measured forces and moments using a five-component balance. The measured balance moments are well matched with the flight test measurements. The shaft moments measured in the wind tunnel test are also plotted together with those values. There is a discrepancy in the roll moments between the balance measurements and the shaft measurements.

Figure 2 shows blade flap hinge rotation angles. The calculated flapping angles are compared with measured values from blades 1 and 2 of both flight and wind tunnel tests. Steady coning from the flight test is lower than that from the wind tunnel test due to a suspected bias error in the flight coning angle measurements [6]. The calculated coning angles for the free flight show good agreement with the LRTA measurements. However, the calculated coning angles for the wind tunnel test show overprediction. The measured longitudinal flapping angles show good agreement between the flight and wind tunnel tests and the calculated longitudinal flapping angles for the wind tunnel test show good correlation with the measurements. The lateral flapping angles from the wind tunnel test are smaller than those from the flight test, and appear consistent with the difference between the balance and shaft moments measured in the wind tunnel test. The calculated lateral flapping angles for flight test show underprediction at all speeds.

CAMRAD II Modeling

The UH-60A Black Hawk in flight was modeled in CAMRAD II [7] as an aircraft with single main and tail rotors. The current model has shown good performance correlation with the flight test data [6] and wind tunnel test data [8]. The trim solution for the flight condition used in CAMRAD II solves for the controls and aircraft attitudes that balance the forces and moments with zero sideslip angle. The horizontal stabilator angle was set to match the measured flight test values from the UH-60A Airloads Program. The trim solution for the wind

tunnel test solves for the controls for the specified thrust and rotor shaft pitch and roll moments.

The aerodynamic model includes a wake analysis to calculate the rotor nonuniform induced-velocities using free wake geometry. The CAMRAD II rotor wake analysis uses second-order lifting line theory, with the general free wake geometry calculation. For loads calculations, a single-peak model was used.

CAMRAD II currently has three free wake models: 1) rolled-up, 2) multiple-trailer, and 3) multiple-trailer with consolidation models. The multiple-trailer and multiple-trailer with consolidation wake models have been recently developed for tiltrotor analysis [5]. Figure 3 shows the calculated wake geometries for $C_w/\sigma = 0.08$ and $\mu = 0.11$. An azimuthal step size of 15 deg was used for the calculation. The rolled-up wake model (Figs. 3(a) and 3(b)) is a typical wake model for a helicopter analysis [9]. A roll-up process is used to model a concentrated tip vortex. The tip vortex strength is determined by the spanwise distribution of bound circulation, and either a single-peak or a dual-peak model can be used depending on the circulation distribution. A large distortion of the tip vortex geometry is observed.

The multiple-trailer wake model has a discrete trailed vortex line emanating from each of the aerodynamic panel edges. The calculations of the free wake geometry in CAMRAD II includes the distortion of all of these trailed lines. Figure 3(c) shows the wake geometries for the multiple-trailer wake model. Only vortex lines from blades at 90 and 270 degree azimuth angle are shown due to complexity of the geometry. A highly concentrated tip vortex is not produced because of the low spanwise resolution and the absence of viscous effects.

The multiple-trailer with consolidation model (Fig. 3(d)) combines the multiple-trailer wake model with a simulation of the tip vortex formation process. With multiple far wake trailed vorticity panels, the trailed lines at the aerodynamic panel edges can be consolidated into rolled-up lines, using the trailed vorticity moment to scale the rate of roll-up. The trailed vorticity is partitioned into sets of adjacent lines that have the same sign (bound circulation increasing and decreasing). For each set, the total strength G, centroid r_C, and moment (radius of gyration) r_G of the trailed vorticity set are calculated:

$$G = \int (-\partial\Gamma/\partial r)\, dr$$

$$Gr_C = \int (-\partial\Gamma/\partial r)\, r\, dr$$

$$Gr_G^2 = \int (-\partial\Gamma/\partial r)\, (r - r_C)^2\, dr$$

where Γ is the bound circulation.

It is assumed that all the vorticity in a set eventually rolls up into a single vortex, located at the centroid of the original vorticity distribution. The characteristic time (r_G^2/Γ) is taken as a measure of the rate of consolidation (See Ref. 5 for more details).

Results and Discussion

The calculated blade section normal force and flap bending moment are compared with the flight and wind tunnel measurements. The analysis uses three wake models: rolled-up, multiple-trailer, and multiple-trailer with consolidation.

Normal Force Correlation

Figures 4 and 5 compare the calculated blade section normal force with the flight test measurements at μ = 0.11 and 0.178 respectively. The section normal force from the flight test was calculated at nine radial stations by integrating chordwise pressure measurements [1]. It contains up to 120 harmonics. The calculations were made using the CAMRAD II analysis with the three free wake models. The analysis has 10 harmonics to describe the blade motion, and an azimuthal step size of 15 deg. A vortex core radius of 20% chord (0.2c) was used for the rolled-up and multiple-trailer wake models. For the rolled-up wake, calculations were made using a tip vortex strength equal to the maximum bound circulation over the span of the blade (complete entrainment). The consolidation model uses a compression form, with linear dependence of the roll-up fraction as wake age and the vortex core radius has a constant value of 80% mean chord.

The measured section normal force exhibits rapid changes near the blade tip due to the interaction of blade with the tip vortices. The airloads near the tip calculated using the rolled-up wake model differ significantly from the measurements. The rolled-up wake shows a region of negative loading on both the advancing and retreating sides at μ = 0.11 and on the advancing side at μ = 0.178. A similar trend was also observed in the previous study [10] using 2GCHAS and CAMRAD/JA. Both multiple-trailer and multiple-trailer with consolidation wake models eliminate the negative loading near the blade tip and qualitatively improve the correlation.

Figures 6 through 9 show the correlation of blade normal force at three different blade span locations for the advance ratios of 0.11, 0.129, 0.149, and 0.178 respectively. The rolled-up wake model shows fair correlation at μ = 0.11. However, the discrepancy between the analysis and measured data near the blade tip and on the advancing side becomes large as the advance

ratio increases. The multiple-trailer wake model shows very weak blade-vortex interaction on the advancing side and overpredicts on the front of the rotor disk at r/R = 0.775. However, it shows fair to good correlation on the front of the rotor disk and retreating side, particularly near the blade tip. The multiple-trailer with consolidation model also shows fair to good correlation on the front of the rotor disk and retreating side, particularly near the blade tip. However, the phase difference on the advancing side is significant.

Figures 10 and 11 compare the cosine and sine harmonics of blade normal force for the advance ratios of 0.11 and 0.178 respectively. The comparisons are made along the blade span for the 1st to 5th harmonics. The scale of y-axis changed for harmonics to better observe the correlation. A significant difference between the wake models occurs at 2/rev, where the rolled-up wake model overpredicts the magnitude from the mid-span to near the tip of a blade. Both the multiple-trailer and multiple-trailer with consolidation models show fair to good correlation on 2/rev magnitude. For the correlation of 3 to 5/rev components, which are important for the prediction of vibration, all three wake models show fair agreement with measurements.

Flap Bending Moment Correlation

Figure 12 compares the oscillatory flap bending moments measured in the flight and wind tunnel tests at C_T/σ of 0.08 for four advance ratios: 0.11, 0.129, 0.149, and 0.178. Flap bending moments were measured at the same nine radial locations along the blade. However, the flight test data shown here do not include the 80% radius values due to a malfunctioning of the strain gauge. The mean values have been removed from both flight and wind tunnel measurements. The flight test data were obtained from measurements over one revolution, and include 1 - 24/rev harmonics and the wind tunnel test data were averaged over 32 revolutions and include 1 - 20/rev harmonics. As expected, the two data sets are similar.

A detailed comparison is shown at three different blade span locations for μ = 0.11 and 0.178 in Fig. 13. The flight test data has 7.5 deg and the wind tunnel test data has 1.5 deg azimuth-resolution. The differences between the flight and wind tunnel tests of the UH-60A rotor fall into two categories: 1) vehicle configuration and 2) aerodynamic condition. In terms of vehicle configuration, the major differences between the flight and wind tunnel tests are the differences in impedance of the hub and control system and effects of the bifilar absorber on the hub. A bifilar absorber was not used in the wind tunnel test. In terms of aerodynamic condition, the differences are the aerodynamic inflow field caused by faired body and wall effects of the wind tunnel. These differences between the flight and wind tunnel tests do not appear to have a significant influence on the oscillatory flap bending moments. The only noticeable difference between the flight and wind tunnel tests was observed at the 70% radius of a blade span. The flight test data contain higher harmonics in the 2nd quadrant and have larger peak-to-peak magnitude. A phase difference was also observed in the 3rd quadrant. Figure 14 shows the comparison of harmonics, 1/rev to 5/rev. The 45 deg diagonal line represents a perfect match between the flight and wind tunnel test data. The harmonics are identified if the difference is larger than 10%. The difference appears for almost all harmonics and the trends are consistent for all advance ratios. However, it is not clear whether these differences are from the differences between flight and wind tunnel test conditions or measurement errors.

Figures 15 and 16 compare the calculated flap bending moment with the flight test measurements at μ = 0.11 and 0.178 respectively. Similar trends were also observed for μ = 0.129 and 0.149. The flap bending moments calculated using the rolled-up wake model differ significantly near the blade root. However, none of these models show good correlation with the measurements. In general, the flap bending moment correlation appears to be worse than the normal force correlation.

Figures 17 and 18 show the correlation of flap bending moment at three different blade span locations for the advance ratio of 0.11 and 0.178 respectively. At all span locations the analysis shows a slight phase lead for the large bending moment in the 4th quadrant. The rolled-up wake model shows a ”bucket” on the advancing side at r/R = 0.5, which appears to result from the large negative airloads on the advancing side. The multiple-trailer wake model does not show significant higher harmonic response. The multiple-trailer with consolidation model shows higher harmonics, but does not appear to improve phase consistently.

Figures 19 and 20 compare the cosine and sine harmonics of flap bending moment along the blade span for the advance ratios of 0.11 and 0.178 respectively. The scale of y-axis changed for harmonics to better observe the correlation. The 3/rev to 5/rev harmonics are greater at μ = 0.11 than μ = 0.178, reflecting the increase in vibration at the transition speed. Unlike the normal force correlation, significant differences between the wake models occur for all harmonic components. The rolled-up wake model overpredicts 1/rev magnitude at the root to mid-span and 2/rev magnitude near the root of a blade, and underpredicts 2/rev magnitude at mid-span. The multiple-trailer with consolidation model shows good

correlation of magnitude for 2/rev component at $\mu = 0.11$ and 1/rev and 2/rev components at $\mu = 0.178$, but exhibits a significant phase difference for the 2/rev component. For the correlation of 3 to 5/rev components, which are important for the prediction of vibration, all three wake models show poor agreement with measurements. The reason for the significant underprediction of the 3/rev cosine component despite the fair correlation of the 3/rev normal force (Figs. 10 and 11) is not known.

The calculated flap bending moments are compared with the wind tunnel measurements at r/R = 0.7 in Fig. 21. The 70% radial location was chosen because a noticeable difference was observed between the flight and wind tunnel test data (Fig. 12). The analysis shows almost same results as the free flight calculation results. Both multiple-trailer and multiple-trailer with consolidation models show fair to good correlation with the measured data. Better correlation with the wind tunnel measurements than with the flight test data has been achieved.

Ascent and Descent Flight

Flight test data were obtained in ascending and descending flight during the Airloads Program. These flight conditions are important for the investigation of the interaction between the blade and the wake. The wake is significantly shifted and the distance between the wake and the rotor disk is affected by flight path angle. Ascents and descents were flown over a ground-acoustic array to obtain acoustic data for a variety of flight path and airspeeds. Airloads and blade dynamic responses were also measured. However, good structural loads data were not obtained due to poor signal conditioning. Two flight conditions were investigated: Flight 95, Counter 9517 and Flight 92, Counter 9223, which correspond to 12.0 deg ascent and 13.5 deg descent flight respectively at $C_w/\sigma = 0.063$ and $\mu = 0.10$.

Normal force is calculated and compared with the flight test data in Figs. 22 and 23. In the ascent flight, tip vortices are convected quickly away from the rotor disk and thus rapid changes of airloads are not observed. All three wake models show significant differences from the flight test data. In general, the interaction of a blade with tip vortices appear to be overpredicted on the advancing side. In the descent flight, high frequency blade-vortex interactions, rapid changes of airloads on the advancing side, and negative loading near the tip were observed. The rolled-up wake model again overpredicts the interaction of a blade with tip vortices on the advancing side. It should be noted that a single-peak model was used for the calculation. Both multiple-trailer and multiple-trailer with consolidation models show better correlation for this flight condition. However, an overprediction is observed on the front of the rotor disk, which results in an underprediction of the 2/rev magnitude. The phase difference on the retreating side is observed for all the wake models.

Shaft Angle Effect in the Wind Tunnel Trim Condition

In wind tunnel, the tip path plane tilt was achieved by varying shaft pitch angle at $C_T/\sigma = 0.08$ and $\mu = 0.1$. The wake is significantly affected by the shaft pitch angles and it is important to investigate the effects of the wake on the structural response. Those test conditions are the wind tunnel test Run 129, Points 9 and 18, which correspond to the shaft angle of -5 deg and $+5$ deg respectively. In this test, the controls were adjusted to zero the 1/rev longitudinal and lateral flapping angles for each shaft angle. Figures 24 and 25 show the correlation of flap bending moment at three different blade span locations for the shaft angle of -5 deg and $+5$ deg respectively. The difference between the two test conditions is considered to be the effect of wake. Significant high frequency components of flap bending moments are observed at r/R = 0.9. However, the measured normal force for the similar test conditions (Figs. 22 and 23) did not contain the same high frequency contents near the blade tip. The multiple-trailer with consolidation wake model shows qualitatively better correlation for $+5$ deg shaft angle.

The cosine and sine harmonic comparison of flap bending moment, shown in Figs. 26 and 27, shows that there is a noticeable difference in 3/rev to 5/rev harmonics between these two flight conditions. Especially the 3/rev magnitude and 5/rev phase show a significant difference. Although the multiple-trailer with consolidation model shows better correlations for some of harmonics for the $+5$ deg shaft angle case, in general none of the wake models are able to capture the changes of flap bending moment due to the shaft angle changes.

Conclusions

The CAMRAD II analysis has been used to predict the normal force and flap bending moment of the full-scale UH-60 Black Hawk helicopter in flight and wind tunnel tests at low speed conditions. The analysis has been conducted using three free wake models: 1) rolled-up, 2) multiple-trailer, and 3) multiple-trailer with consolidation wake models. The results have been correlated with the test data for several different flight and wind tunnel test conditions.

From this study the following conclusions are obtained:

1. There is good agreement for the oscillatory flap bending moments between the flight and wind tunnel tests when the rotor in the wind tunnel was trimmed to match the thrust and pitch and roll moments measured on the main rotor shaft in the flight test. The differences between the flight and wind tunnel tests of the UH-60A rotor, such as the impedance of the hub and control system, wall effects in the wind tunnel, and bifilar hub absorber, do not have a significant influence on the oscillatory flap bending moments.

2. Both multiple-trailer and multiple-trailer with consolidation models eliminate the negative loading near the blade tip, which was observed using the rolled-up wake model, and improve the normal force correlation qualitatively.

3. The multiple-trailer with consolidation model shows good correlation of flap bending moments for 2/rev magnitude at $\mu = 0.11$ and 1/rev and 2/rev magnitudes at $\mu = 0.178$. However, for the correlation of 3/rev to 5/rev harmonics, which are important for the prediction of vibration, all three wake models show poor agreement with measurements.

4. The comparison of calculations with the ascent flight data shows that all the wake models appear to overpredict the interaction of a blade with tip vortices on the advancing side. Both multiple-trailer and multiple-trailer with consolidation models show better correlation than the rolled-up wake in the descent flight.

5. There is a significant change in the 3/rev and 5/rev flap bending moments between forward and backward shaft tilts as measured in the wind tunnel. However, the analysis was not able to capture these differences.

Acknowledgment

The authors would like to acknowledge the efforts of the UH-60/LRTA test team in the conduct of the test program.

References

[1] Kufeld, R. M., Balough, D. L., Cross, J. L., Studebaker, K. F., Jennison, C. D., and Bousman, W. G., "Flight Testing of the UH-60A Airloads Aircraft," American Helicopter Society 50th Annual Forum Proceedings, Washington D.C., May 1994.

[2] Norman, T. R, Shinoda, P. M., Kitaplioglu, C., Jacklin, S. A., and Sheikman, A., "Low-Speed Wind Tunnel Investigation of a Full-Scale UH-60 Rotor System," American Helicopter Society 58th Annual Forum Proceedings, Montreal, Canada, June 2002.

[3] Bousman, W. G., and Maier, T. H., "An Investigation of Helicopter Rotor Blade Flap Vibratory Loads," American Helicopter Society 48th Annual Forum Proceedings, Washington, D.C., June 1992.

[4] Johnson, W., "Calculation of Tilt Rotor Aeroacoustic Model (TRAM DNW) Performance, Airloads, and Structural Loads," American Helicopter Society Aeromechanics Specialist Meeting Proceedings, Atlanta, GA, November 2000.

[5] Johnson, W., "Influence of Wake Models on Calculated Tiltrotor Aerodynamics," American Helicopter Society Aerodynamics, Acoustics , and Test and Evaluation Technical Specialist Meeting Proceedings, San Francisco, CA, January 2002.

[6] Yeo, H., Bousman, W. G., and Johnson, W., "Performance Analysis of a Utility Helicopter with Standard and Advanced Rotors," American Helicopter Society Aerodynamics, Acoustics , and Test and Evaluation Technical Specialist Meeting Proceedings, San Francisco, CA, January 2002.

[7] Johnson, W., "Rotorcraft Aerodynamics Models for a Comprehensive Analysis," American Helicopter Society 54th Annual Forum Proceedings, Washington, D.C., May 1998.

[8] Shinoda, P. M., Yeo, H., and Norman, T. R., "Rotor Performance of a UH-60 Rotor System in the NASA Ames 80- by 120- Foot Wind Tunnel," American Helicopter Society 58th Annual Forum Proceedings, Montreal, Canada, June 2002.

[9] Johnson, W., "A General Free Wake Geometry Calculation for Wings and Rotors," American Helicopter Society 51st Annual Forum Proceedings, Forth Worth, TX, May 1995.

[10] Lim, J. W., "Analytical Investigation of UH-60A Flight Blade Airloads and Loads Data," American Helicopter Society 51st Annual Forum Proceedings, Fort Worth, TX, May 1995.

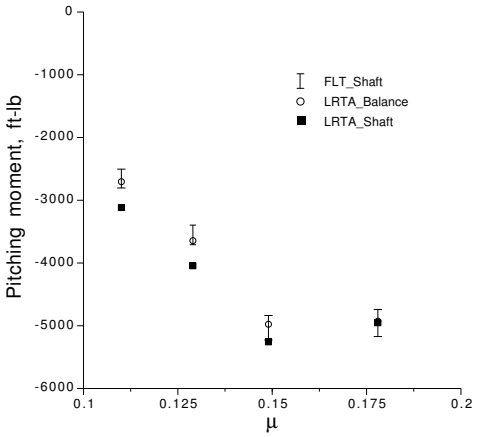

(a) Pitching moment

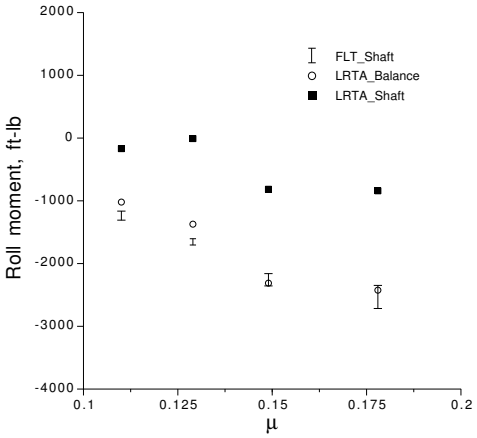

(b) Roll moment

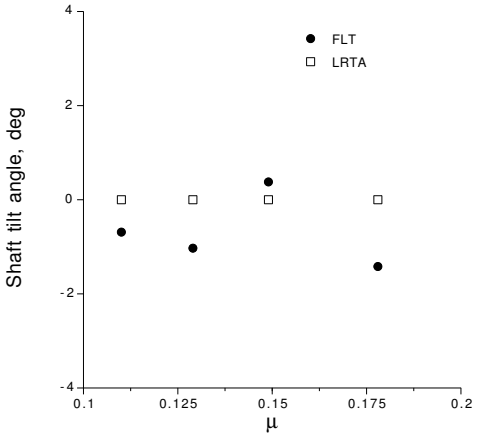

(c) Shaft angle

Fig. 1 Flight and LRTA wind tunnel test trim conditions

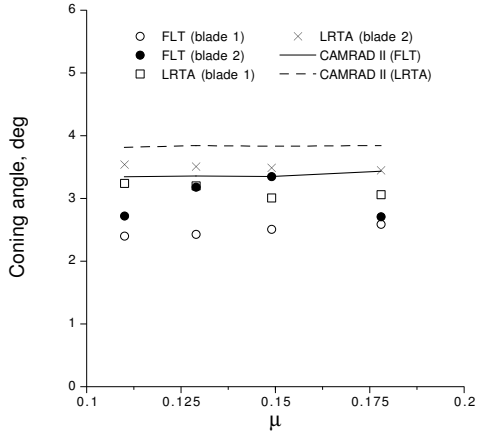

(a) Coning angle

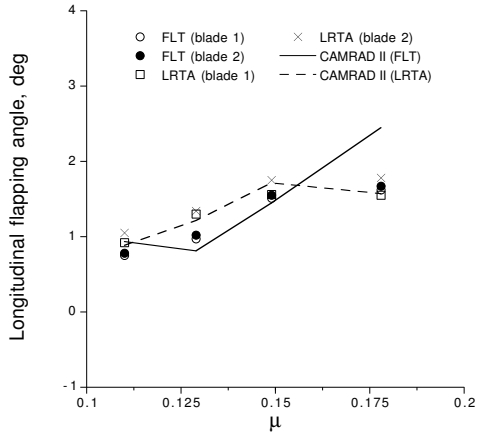

(b) Longitudinal flapping angle

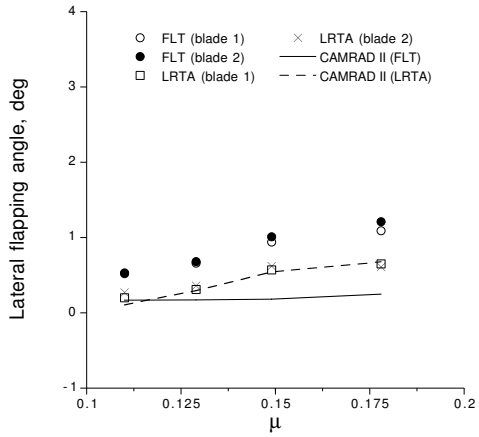

(c) lateral flapping angle

Fig. 2 Flight test versus LRTA wind tunnel test: flapping angle

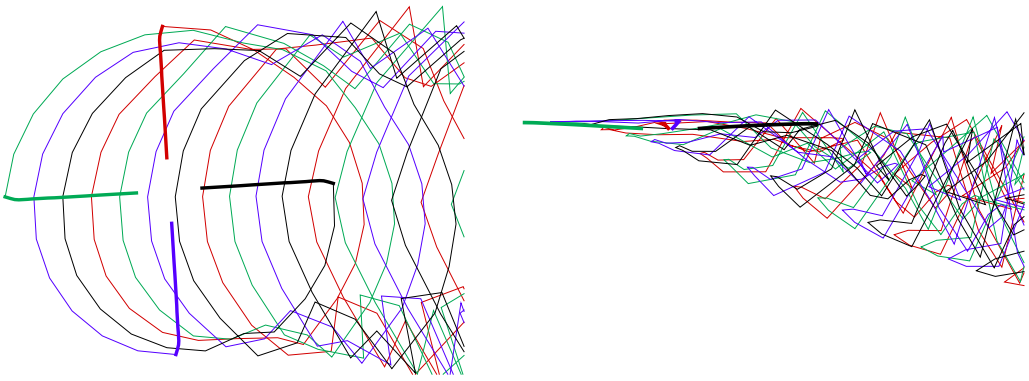

(a) Rolled-up wake (Top view)

(b) Rolled-up wake (Side view)

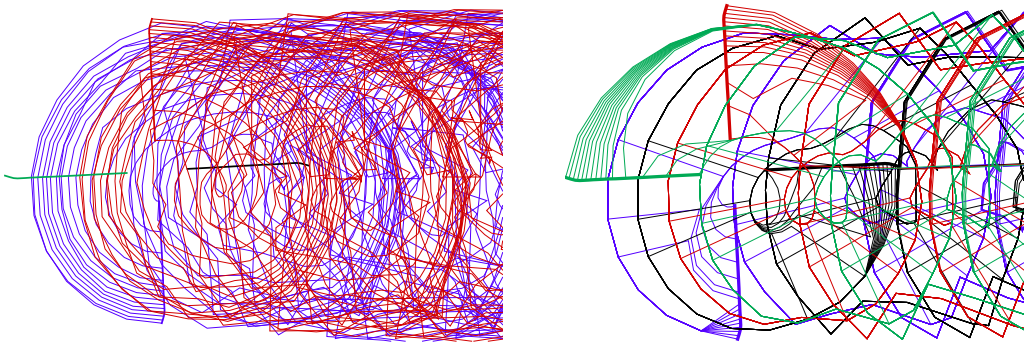

(c) Multiple-trailer wake

(d) Multiple-trailer with consolidation

Fig. 3 Calculated wake geometry for flight, $C_w/\sigma = 0.08$, $\mu = 0.11$

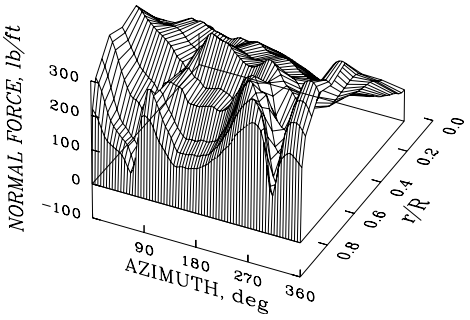

(a) Flight test

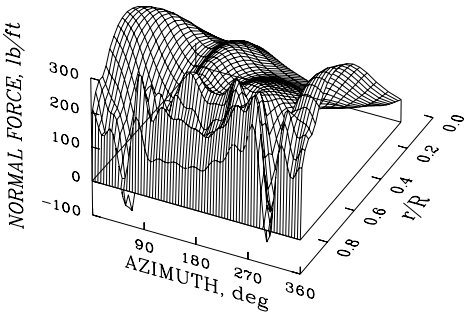

(b) Rolled-up wake

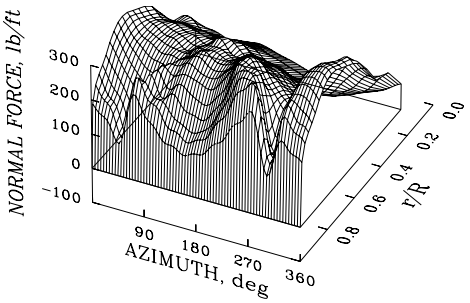

(c) Multiple-trailer wake

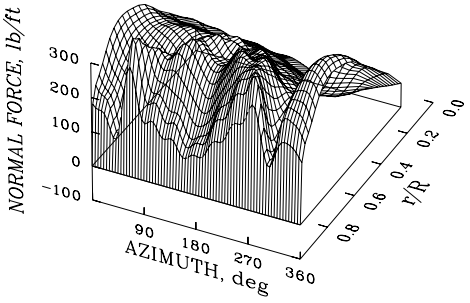

(d) Multiple-trailer with consolidation

Fig. 4 Comparison of blade section normal force with flight test for $\mu = 0.11$

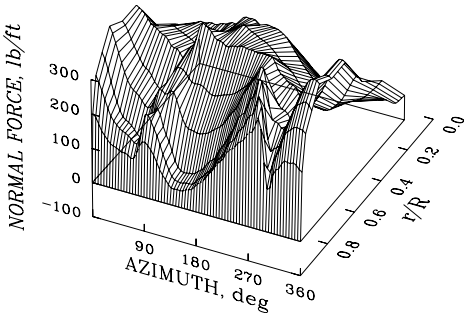

(a) Flight test

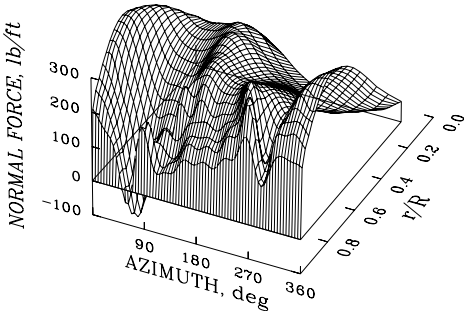

(b) Rolled-up wake

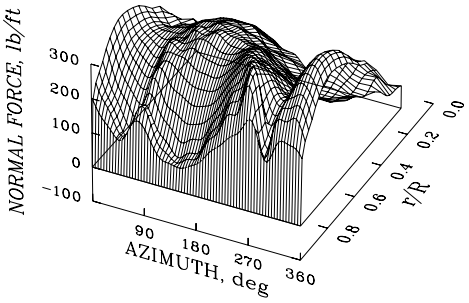

(c) Multiple-trailer wake

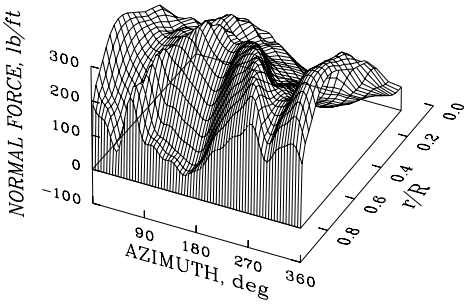

(d) Multiple-trailer with consolidation

Fig. 5 Comparison of blade section normal force with flight test for $\mu = 0.178$

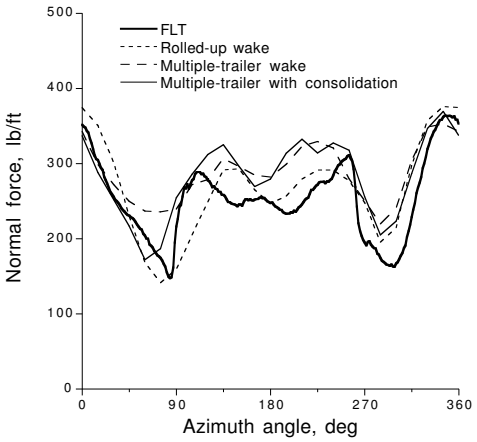

(a) r/R = 0.775

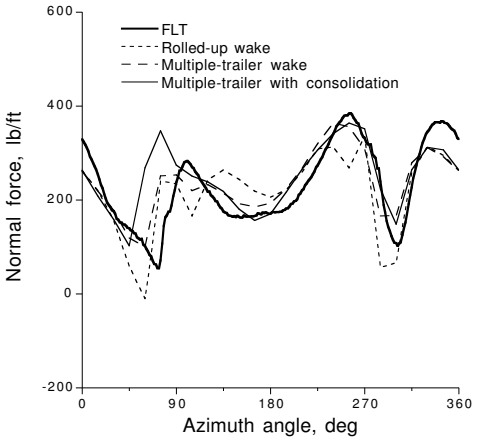

(b) r/R = 0.92

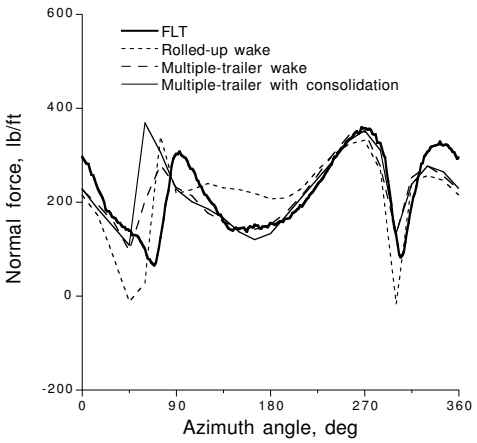

(c) r/R = 0.965

Fig. 6 Correlation of normal force with flight test data for $\mu = 0.11$

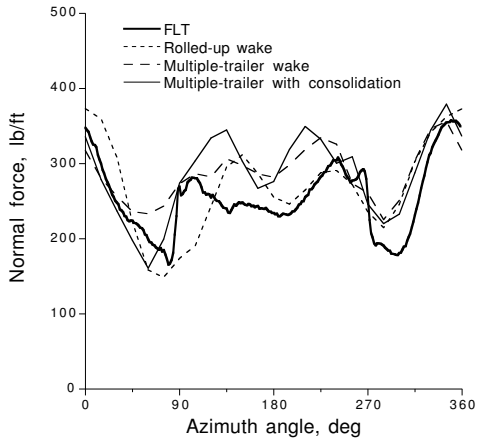

(a) r/R = 0.775

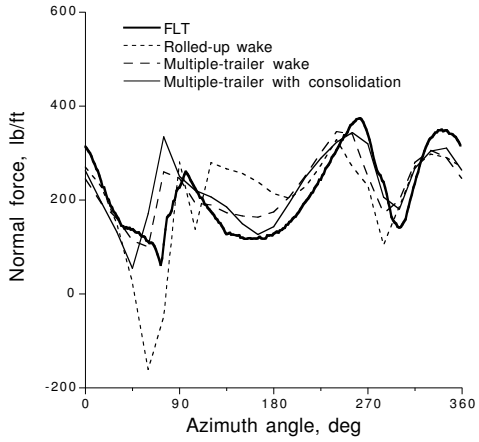

(b) r/R = 0.92

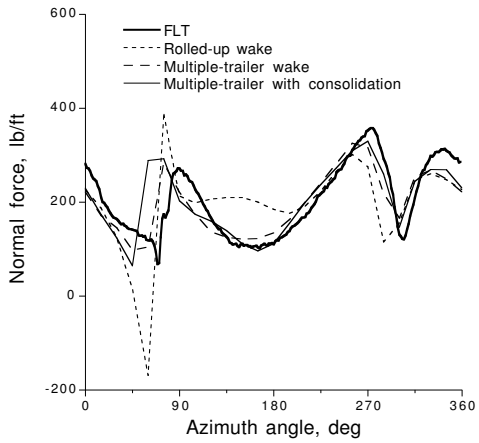

(c) r/R = 0.965

Fig. 7 Correlation of normal force with flight test data for $\mu = 0.129$

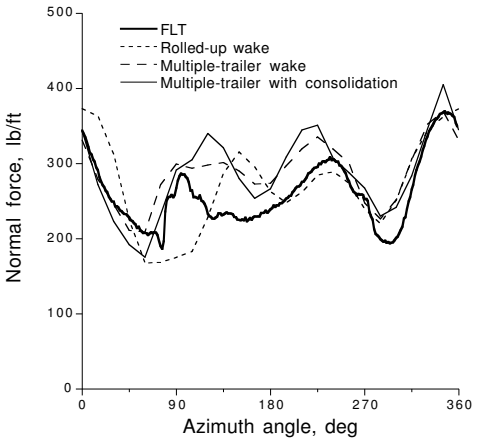

(a) r/R = 0.775

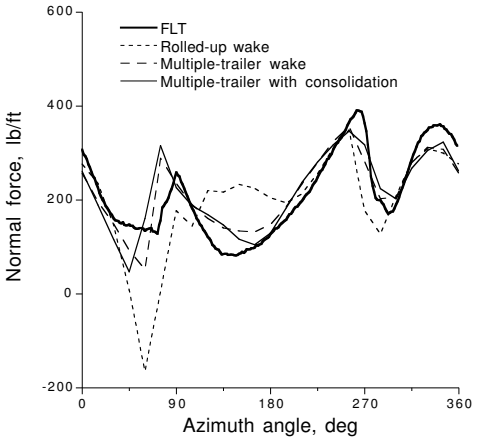

(b) r/R = 0.92

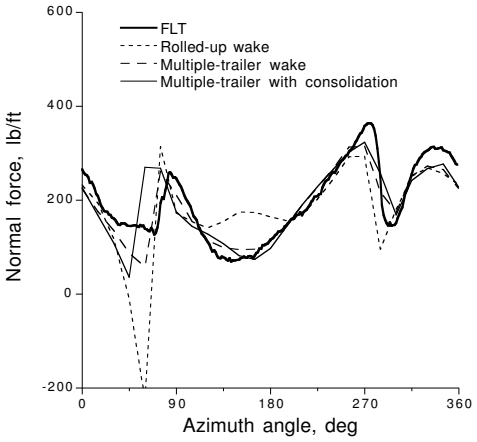

(c) r/R = 0.965

Fig. 8 Correlation of normal force with flight test data for $\mu = 0.149$

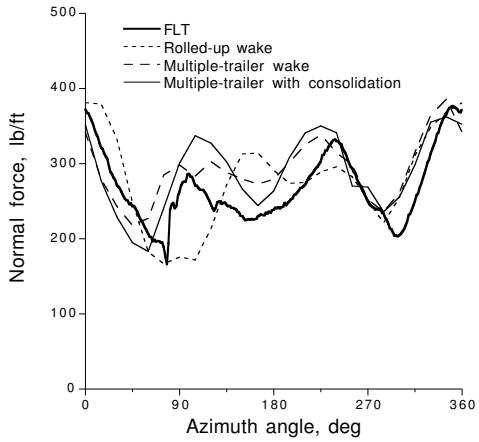

(a) r/R = 0.775

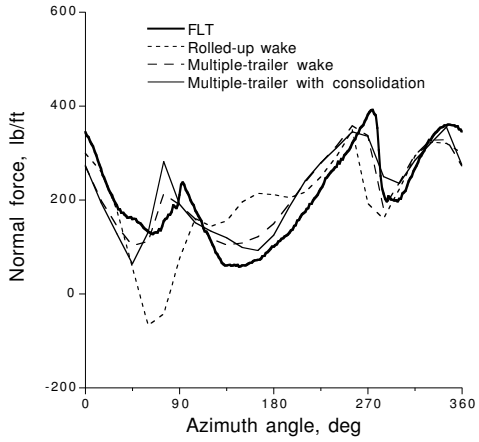

(b) r/R = 0.92

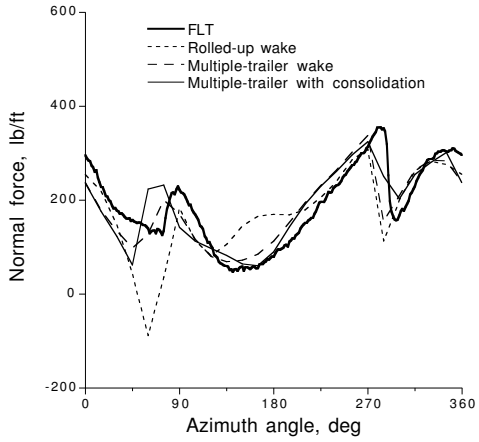

(c) r/R = 0.965

Fig. 9 Correlation of normal force with flight test data for $\mu = 0.178$

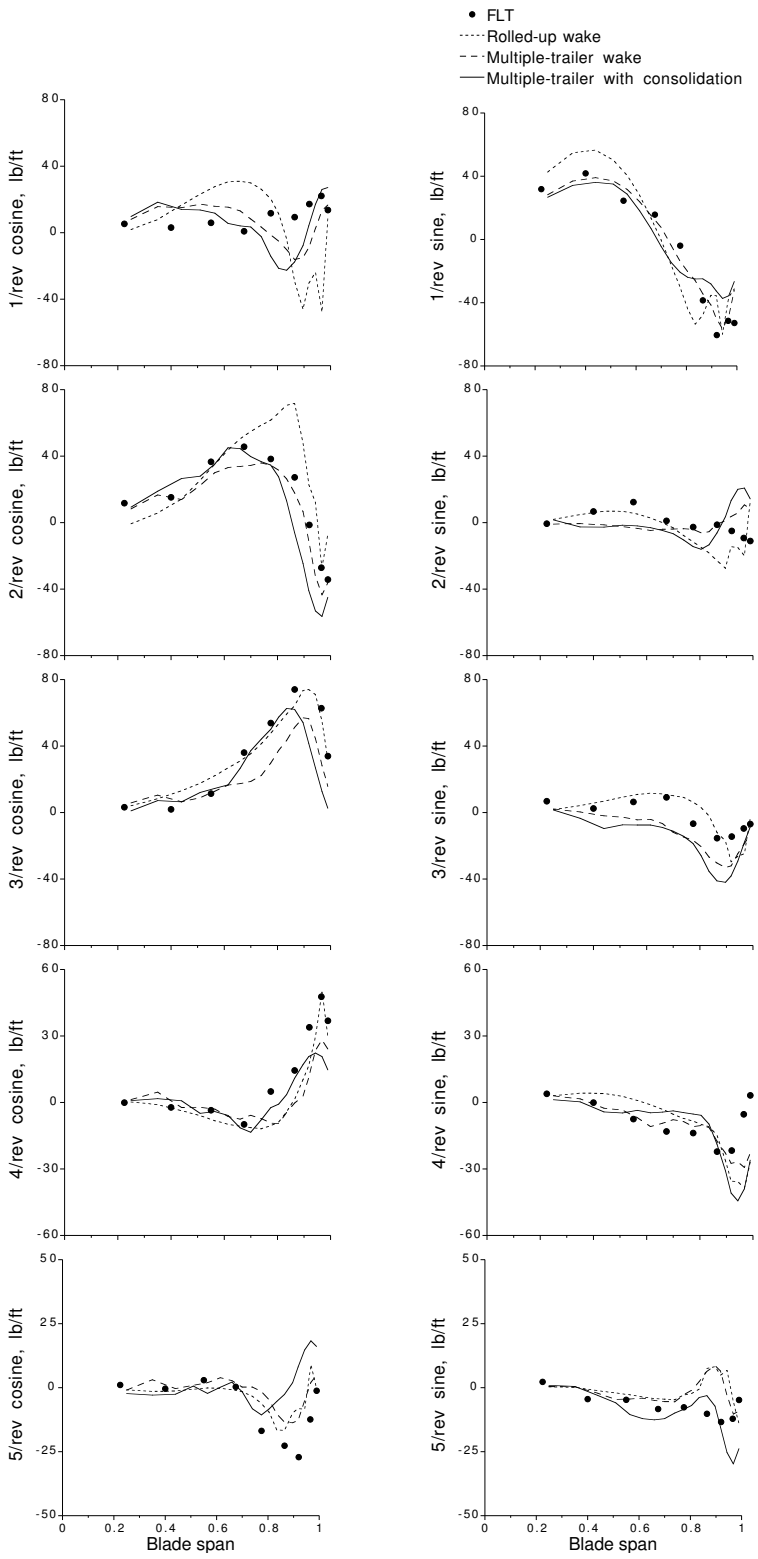

Fig. 10 Comparison of cosine and sine harmonics of normal force with flight test data for $\mu = 0.11$

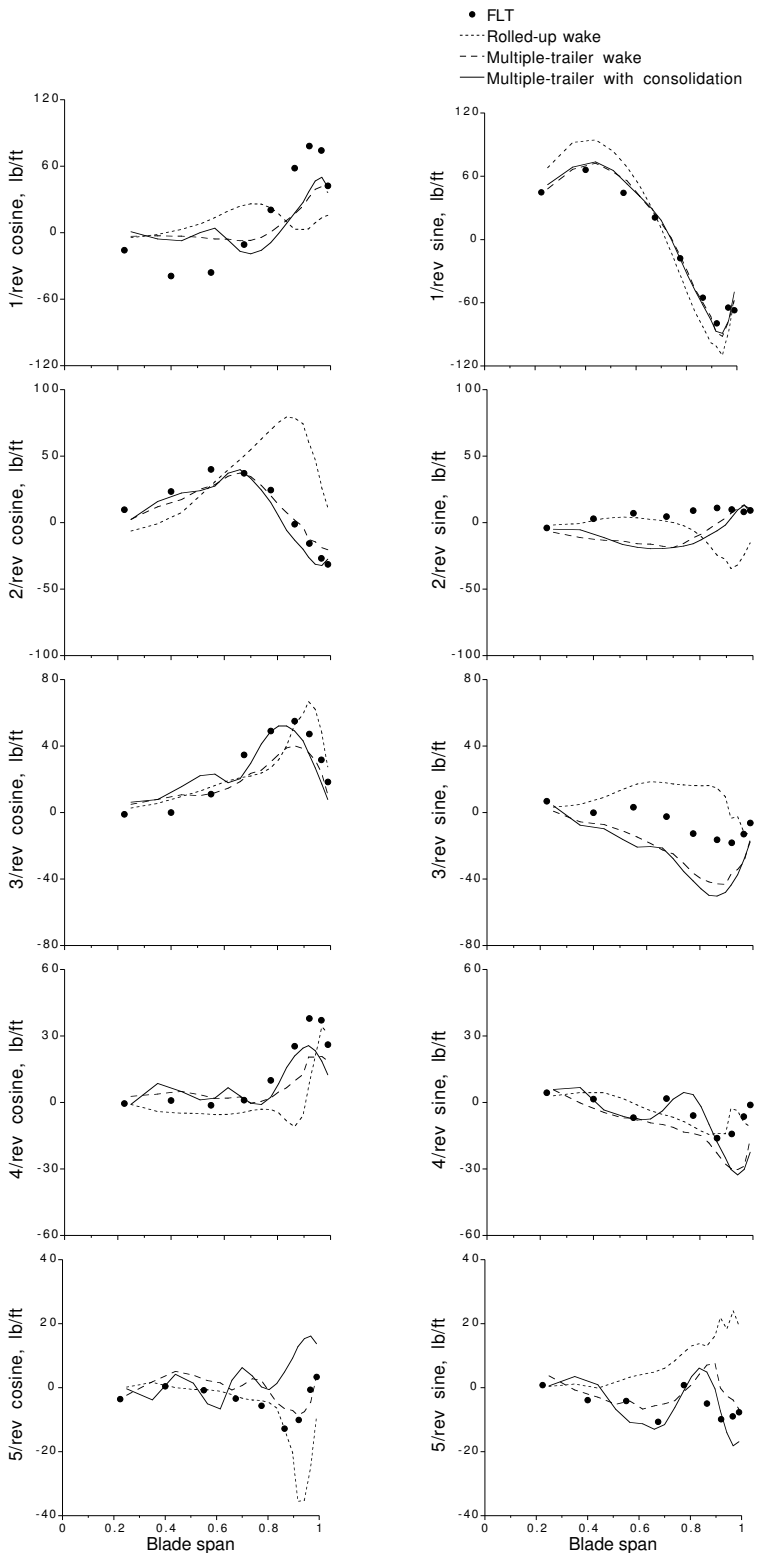

Fig. 11 Comparison of cosine and sine harmonics of normal force with flight test data for $\mu = 0.178$

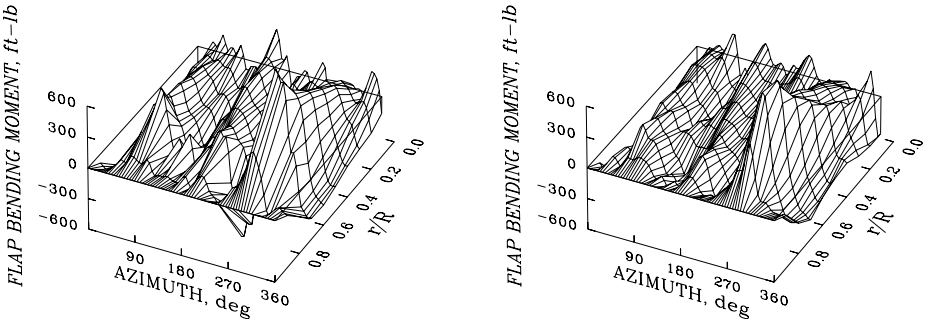

(a) Flight test, $\mu = 0.110$

(b) Wind tunnel test, $\mu = 0.110$

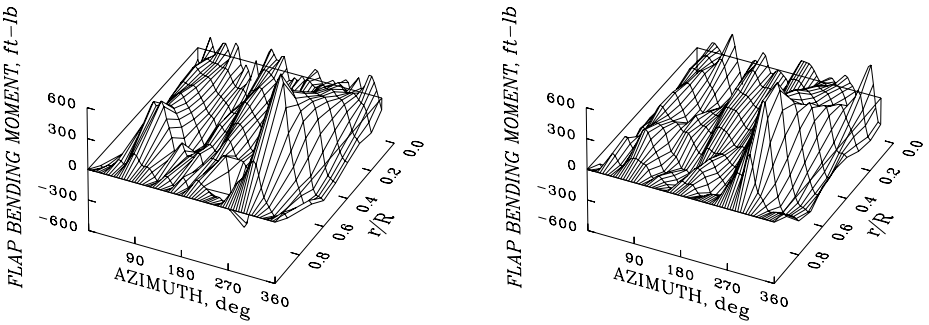

(c) Flight test, $\mu = 0.129$

(d) Wind tunnel test, $\mu = 0.129$

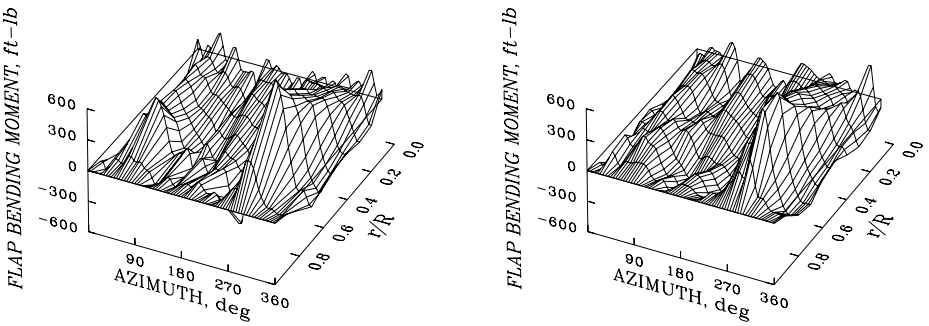

(e) Flight test, $\mu = 0.149$

(f) Wind tunnel test, $\mu = 0.149$

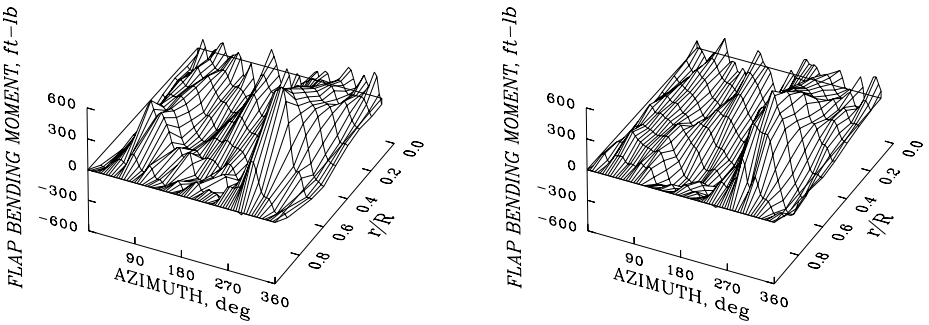

(g) Flight test, $\mu = 0.178$

(h) Wind tunnel test, $\mu = 0.178$

Fig. 12 Comparison of oscillatory flap bending moment between flight and wind tunnel test for $C_T/\sigma = 0.08$

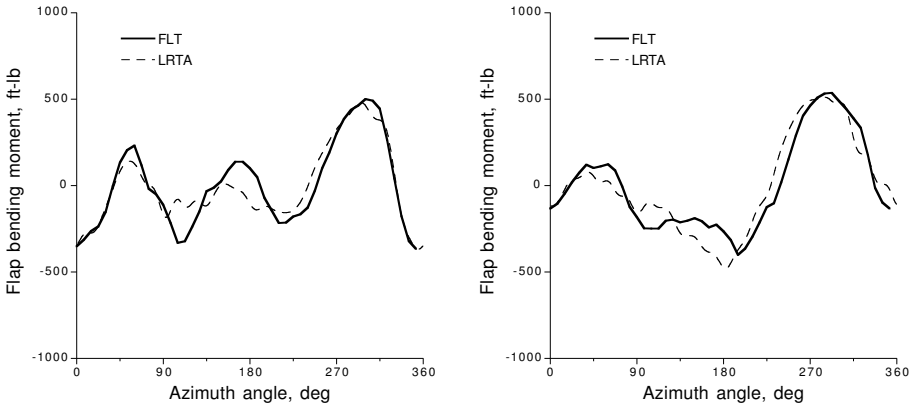

(a) $\mu = 0.11$, r/R = 0.5

(b) $\mu = 0.178$, r/R = 0.5

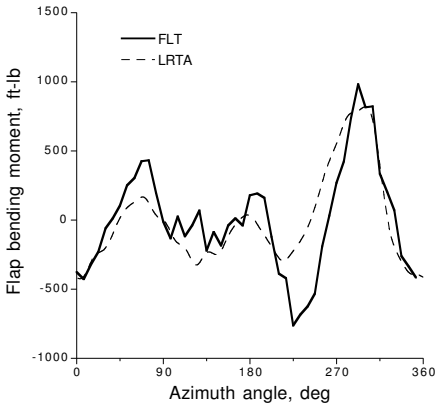

(c) $\mu = 0.11$, r/R = 0.7

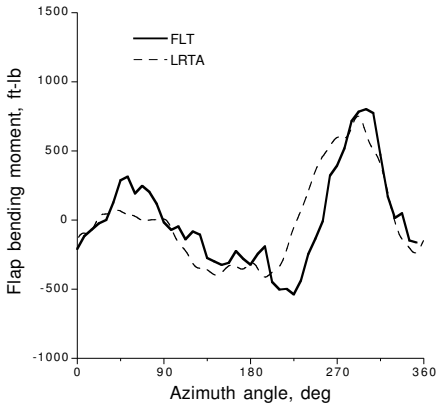

(d) $\mu = 0.178$, r/R = 0.7

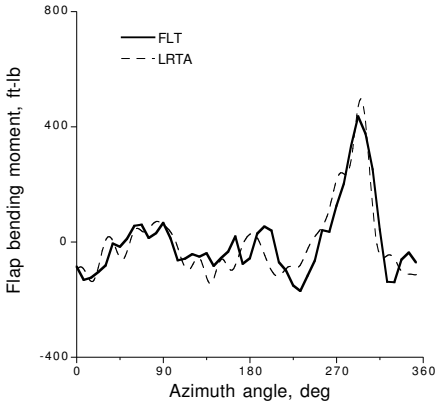

(e) $\mu = 0.11$, r/R = 0.9

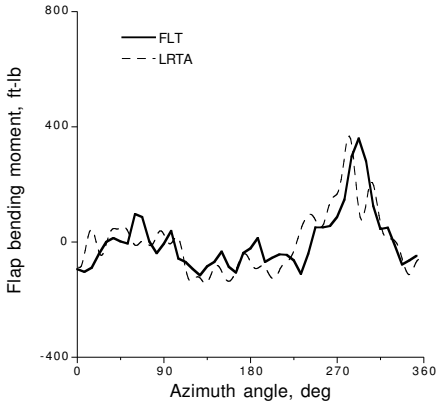

(f) $\mu = 0.178$, r/R = 0.9

Fig. 13 Comparison of oscillatory flap bending moment between flight and wind tunnel test

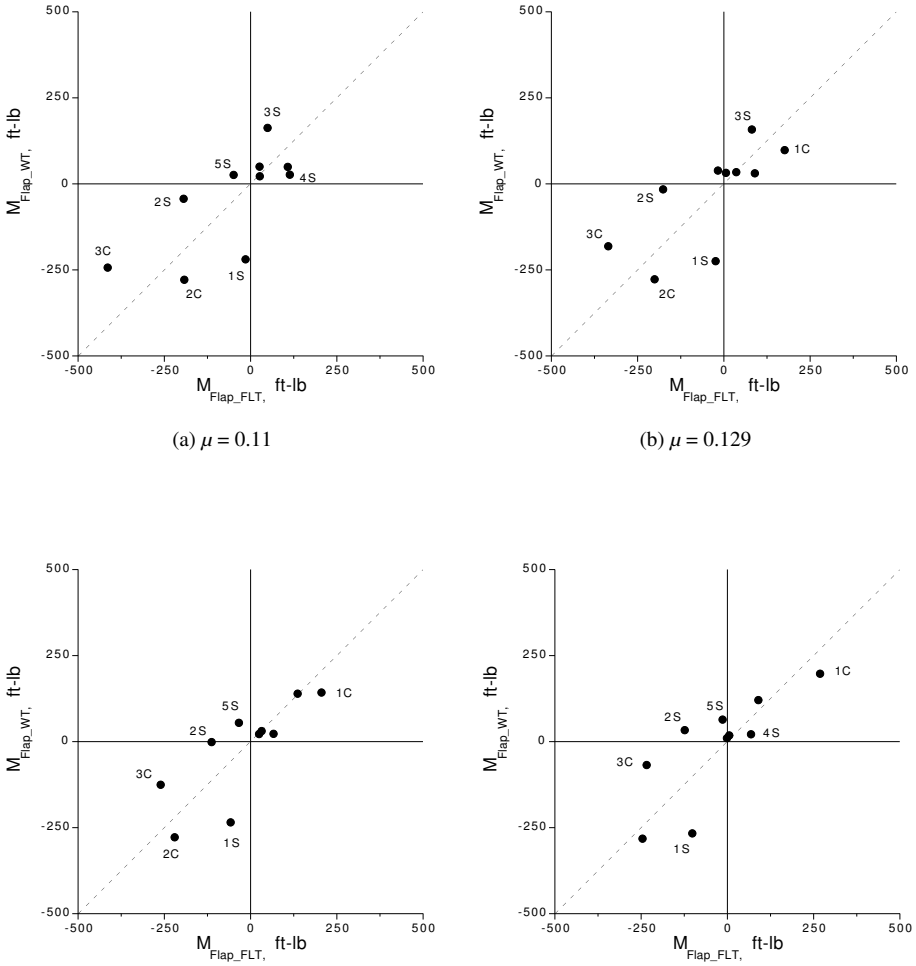

(a) $\mu = 0.11$

(b) $\mu = 0.129$

(c) $\mu = 0.149$

(d) $\mu = 0.178$

Fig. 14 Harmonic comparison of flap bending moment between flight and wind tunnel test at r/R = 0.7

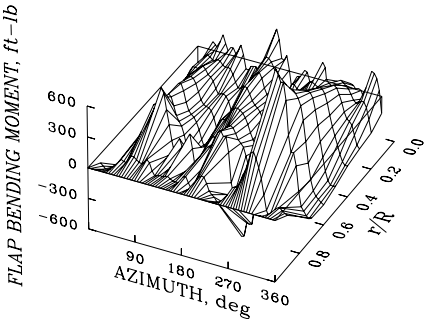

(a) Flight test

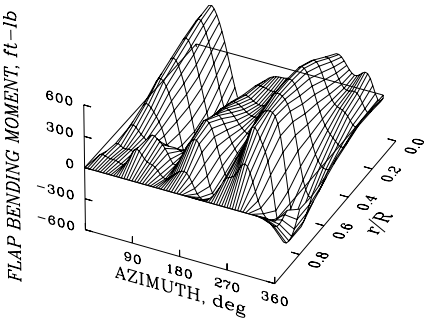

(b) Rolled-up wake

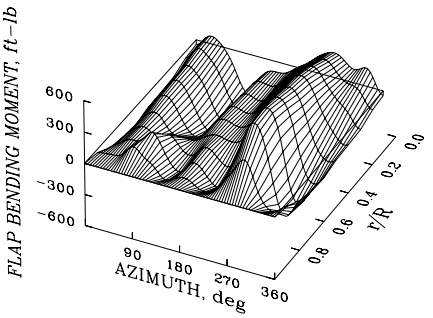

(c) Multiple-trailer wake

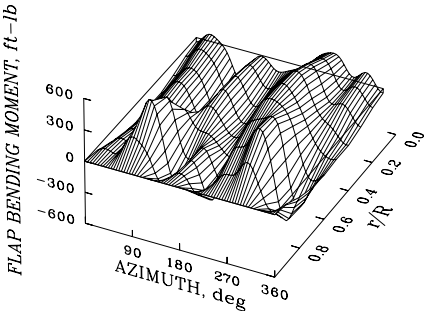

(d) Multiple-trailer with consolidation

Fig. 15 Comparison of oscillatory flap bending moment with flight test for $\mu = 0.11$

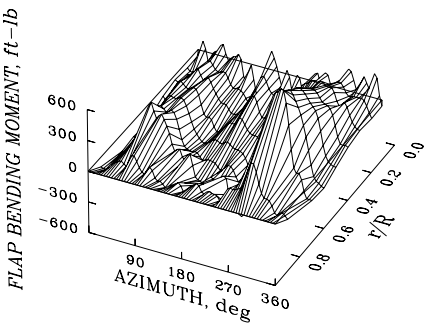

(a) Flight test

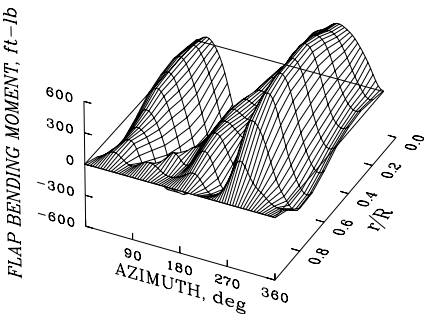

(b) Rolled-up wake

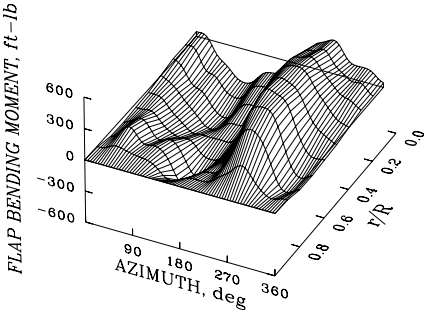

(c) Multiple-trailer wake

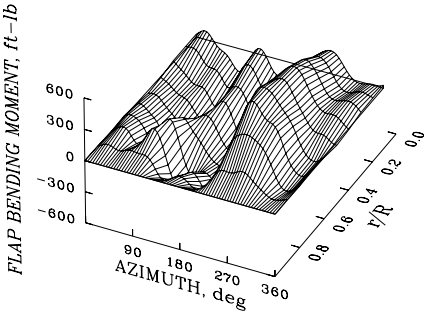

(d) Multiple-trailer with consolidation

Fig. 16 Comparison of oscillatory flap bending moment with flight test for $\mu = 0.178$

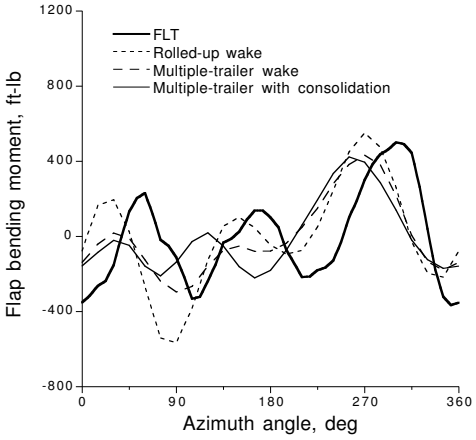

(a) r/R = 0.5

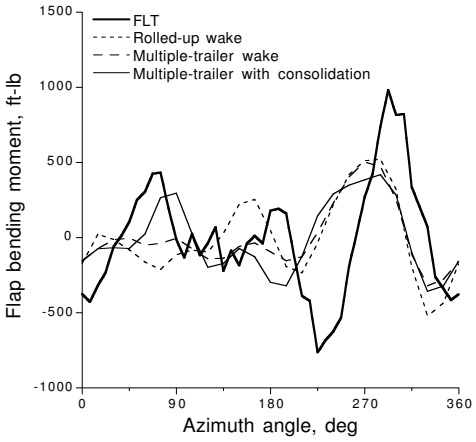

(b) r/R = 0.7

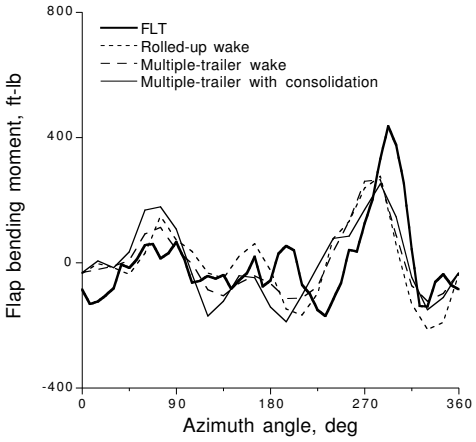

(c) r/R = 0.9

Fig. 17 Correlation of oscillatory flap bending moment with flight test data for $\mu = 0.11$

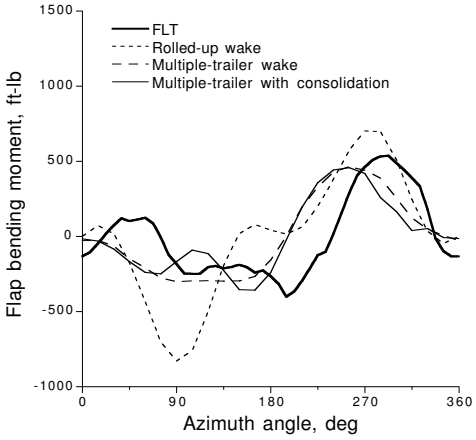

(a) r/R = 0.5

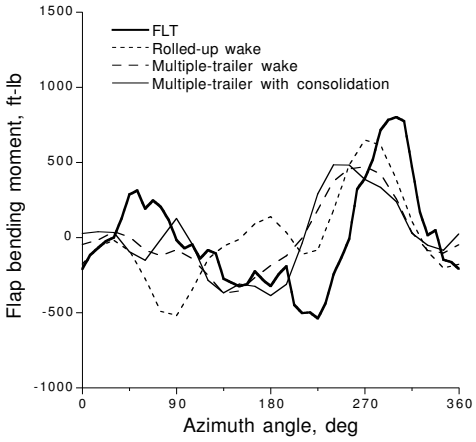

(b) r/R = 0.7

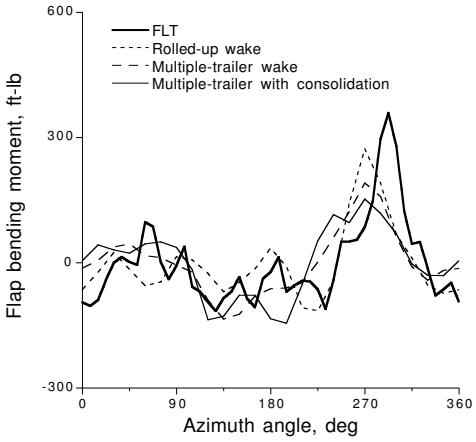

(c) r/R = 0.9

Fig. 18 Correlation of oscillatory flap bending moment with flight test data for $\mu = 0.178$

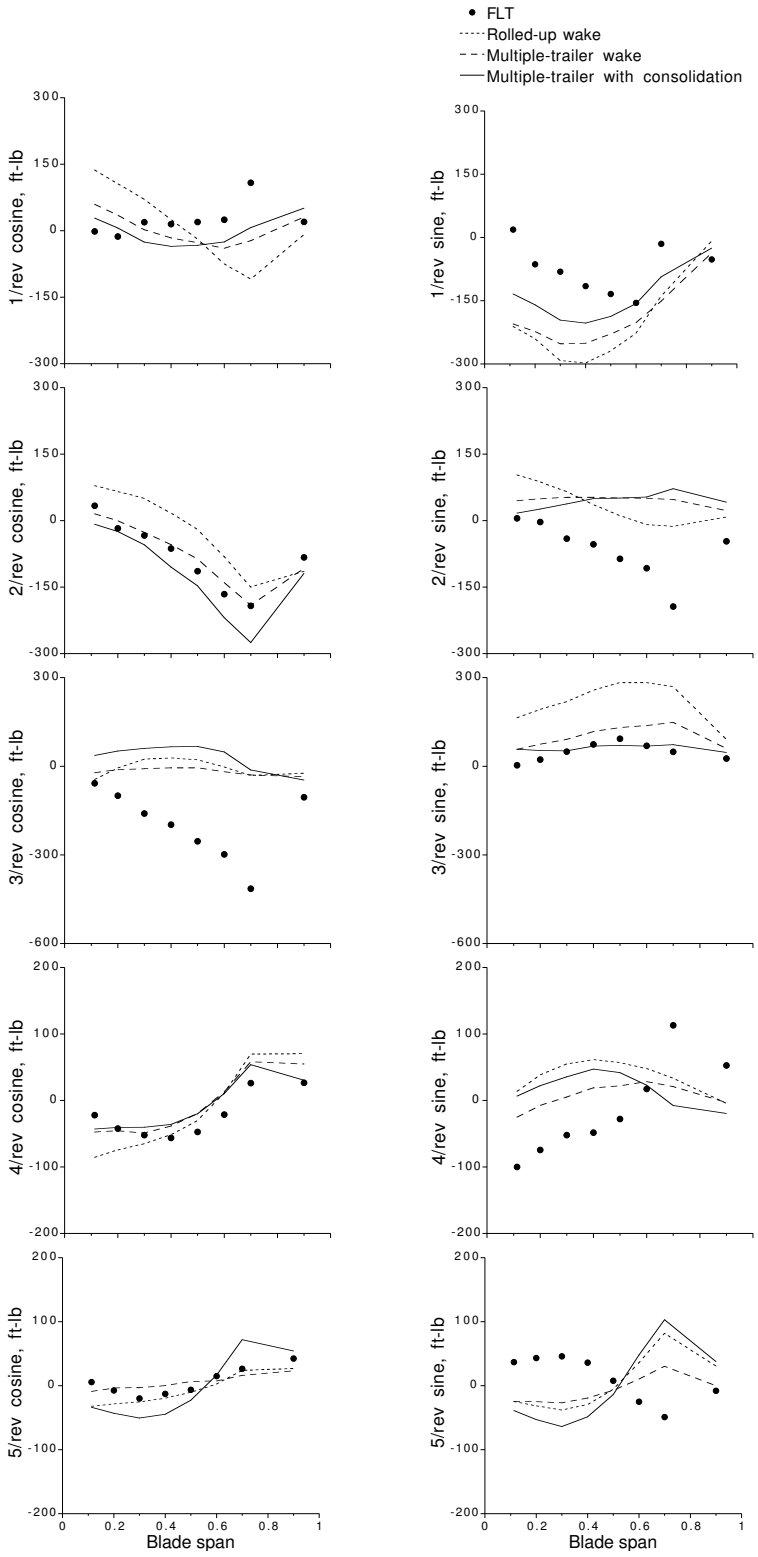

Fig. 19 Comparison of cosine and sine harmonics of flap bending moment with flight test data for $\mu = 0.11$

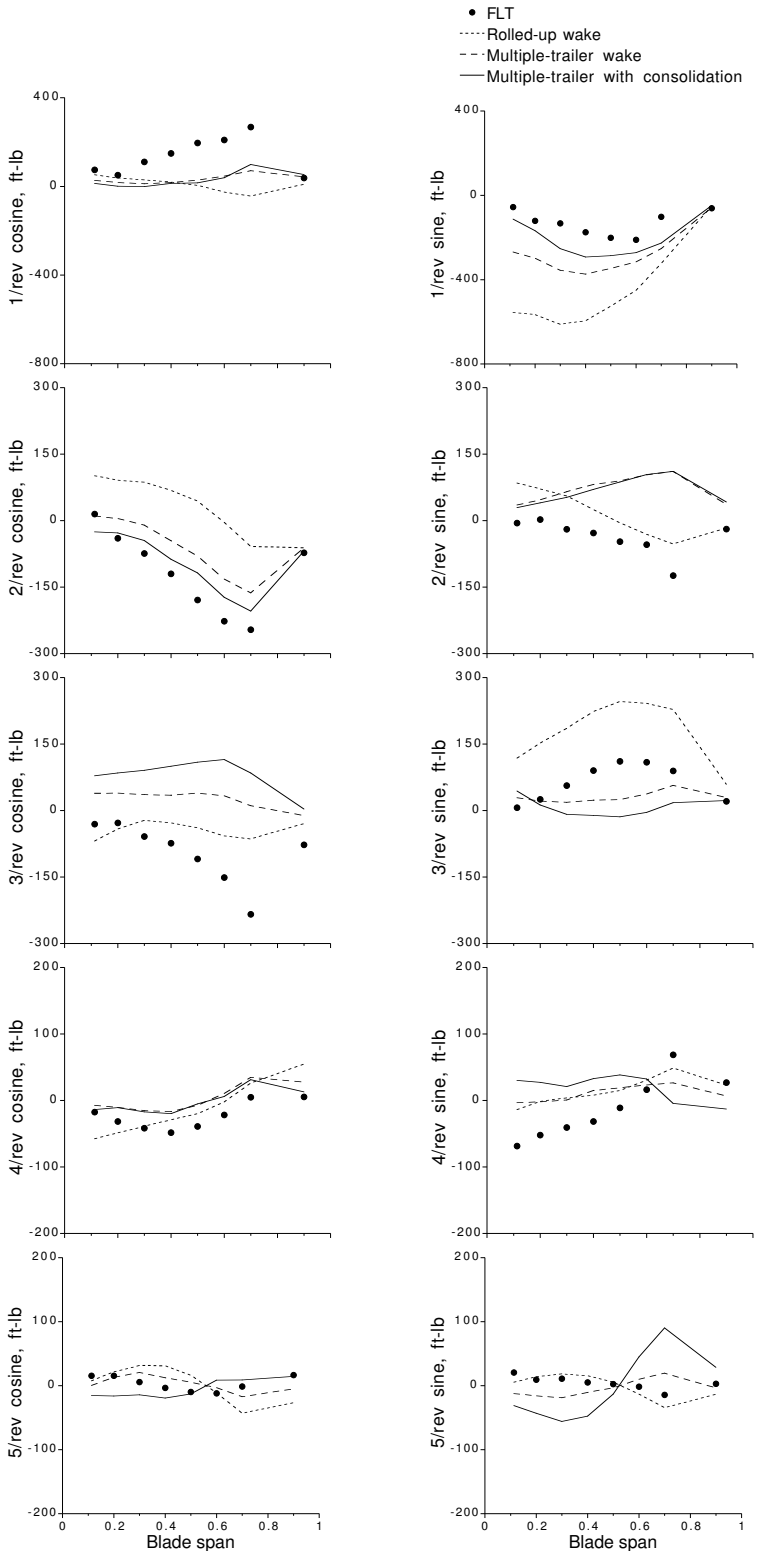

Fig. 20 Comparison of cosine and sine harmonics of flap bending moment with flight test data for $\mu = 0.178$

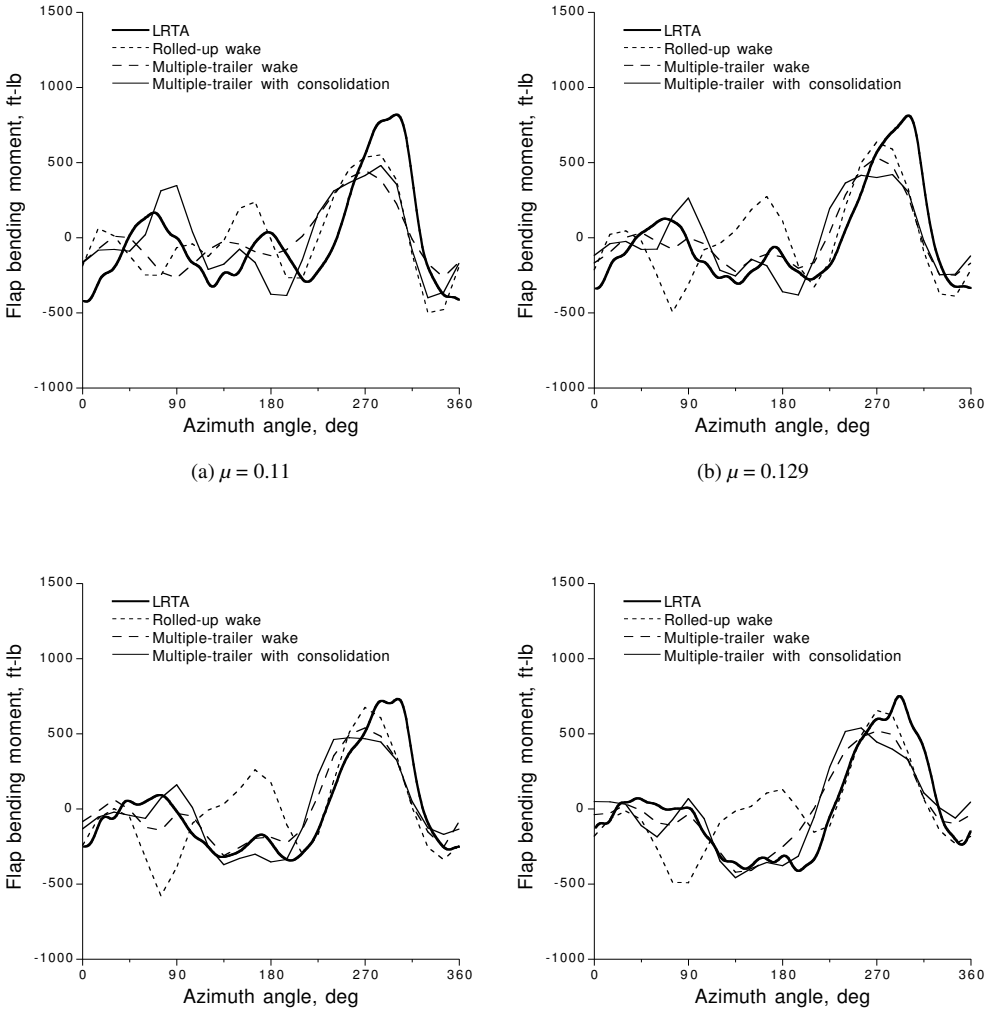

(a) $\mu = 0.11$

(b) $\mu = 0.129$

(c) $\mu = 0.149$

(d) $\mu = 0.178$

Fig. 21 Correlation of oscillatory flap bending moment with wind tunnel test data at r/R = 0.7

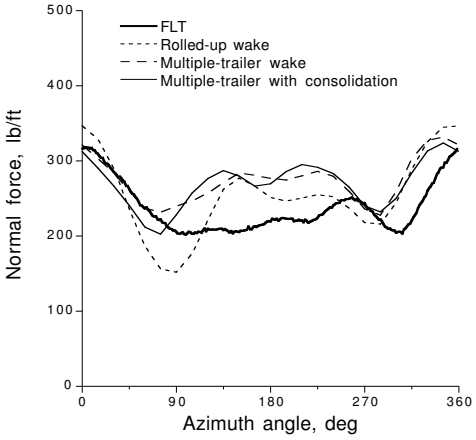

(a) r/R = 0.775

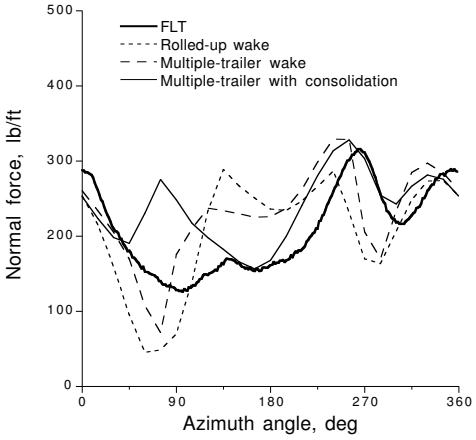

(b) r/R = 0.92

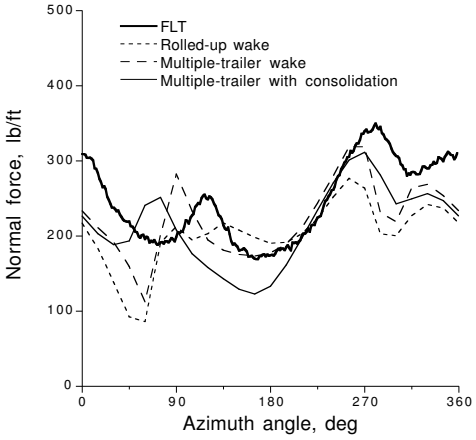

(c) r/R = 0.965

Fig. 22 Correlation of normal force with ascent flight test data for $C_w/\sigma = 0.063$, $\mu = 0.10$, $\gamma = +12.0$ deg

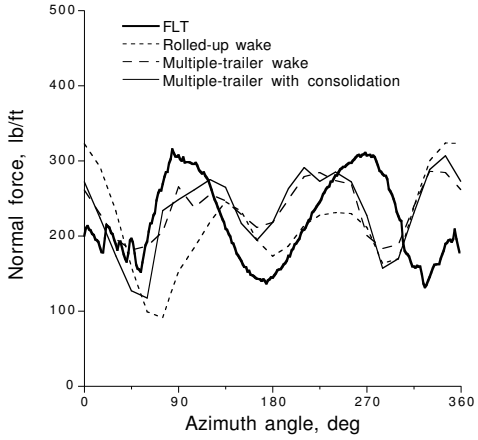

(a) r/R = 0.775

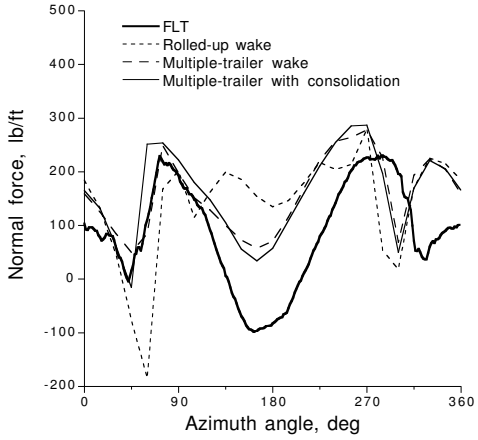

(b) r/R = 0.92

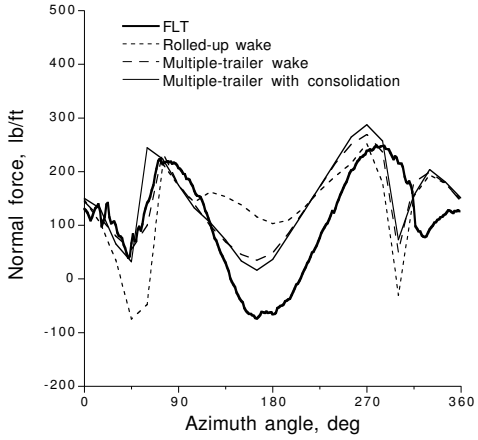

(c) r/R = 0.965

Fig. 23 Correlation of normal force with descent flight test data for $C_w/\sigma = 0.063$, $\mu = 0.10$, $\gamma = -13.5$ deg

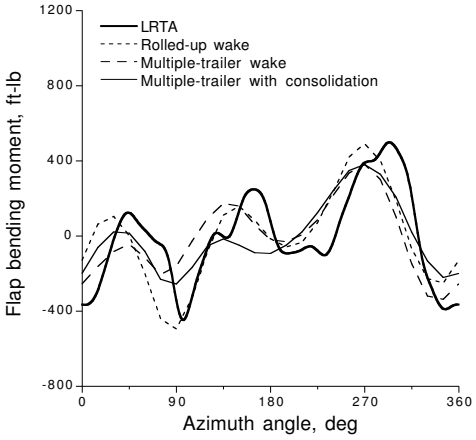

(a) r/R = 0.5

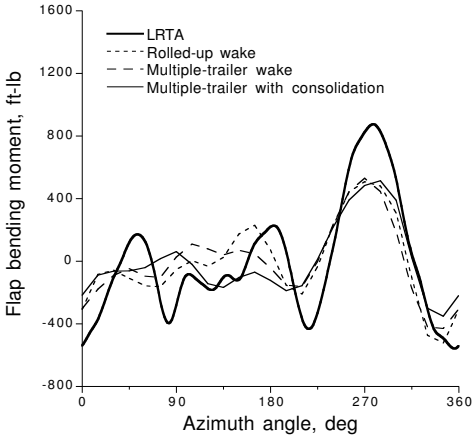

(b) r/R = 0.7

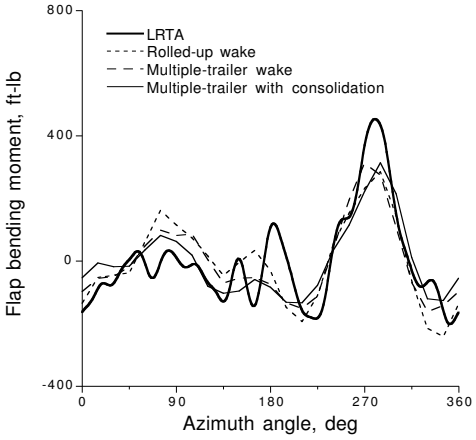

(c) r/R = 0.9

Fig. 24 Correlation of oscillatory flap bending moment with wind tunnel test data for $C_T/\sigma = 0.08$, $\mu = 0.10$, shaft pitch = -5.0 deg

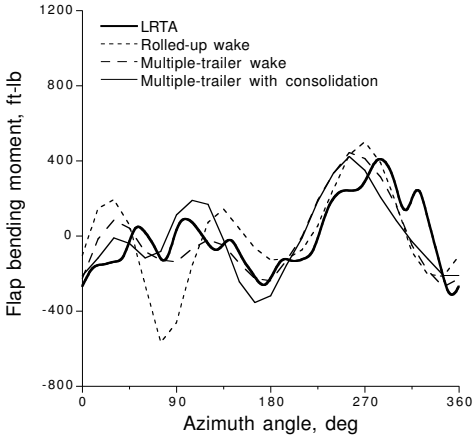

(a) r/R = 0.5

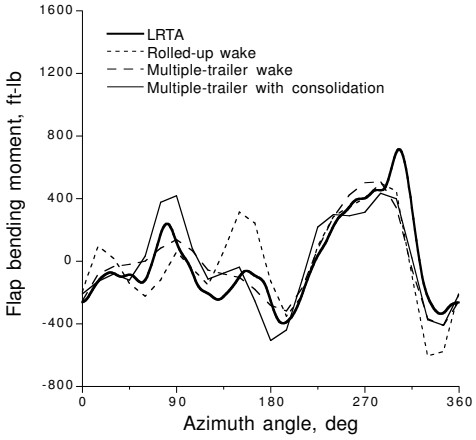

(b) r/R = 0.7

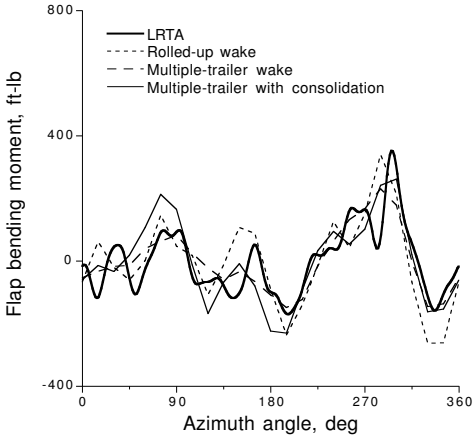

(c) r/R = 0.9

Fig. 25 Correlation of oscillatory flap bending moment with wind tunnel test data for $C_T/\sigma = 0.08$, $\mu = 0.10$, shaft pitch = $+5.0$ deg

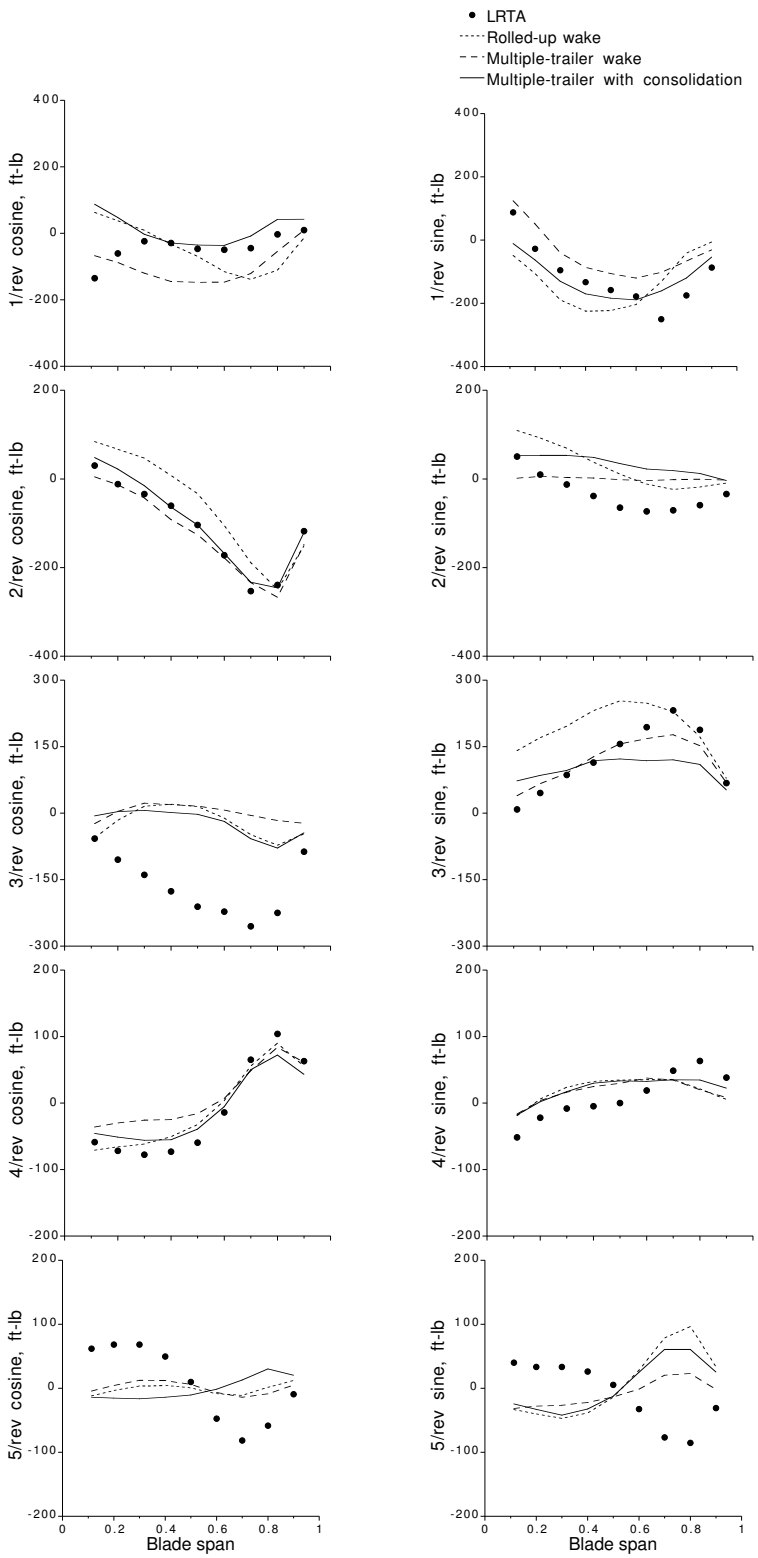

Fig. 26 Comparison of cosine and sine harmonics of flap bending moment with wind tunnel test data for $C_T/\sigma = 0.08$, $\mu = 0.10$, shaft pitch = -5.0 deg

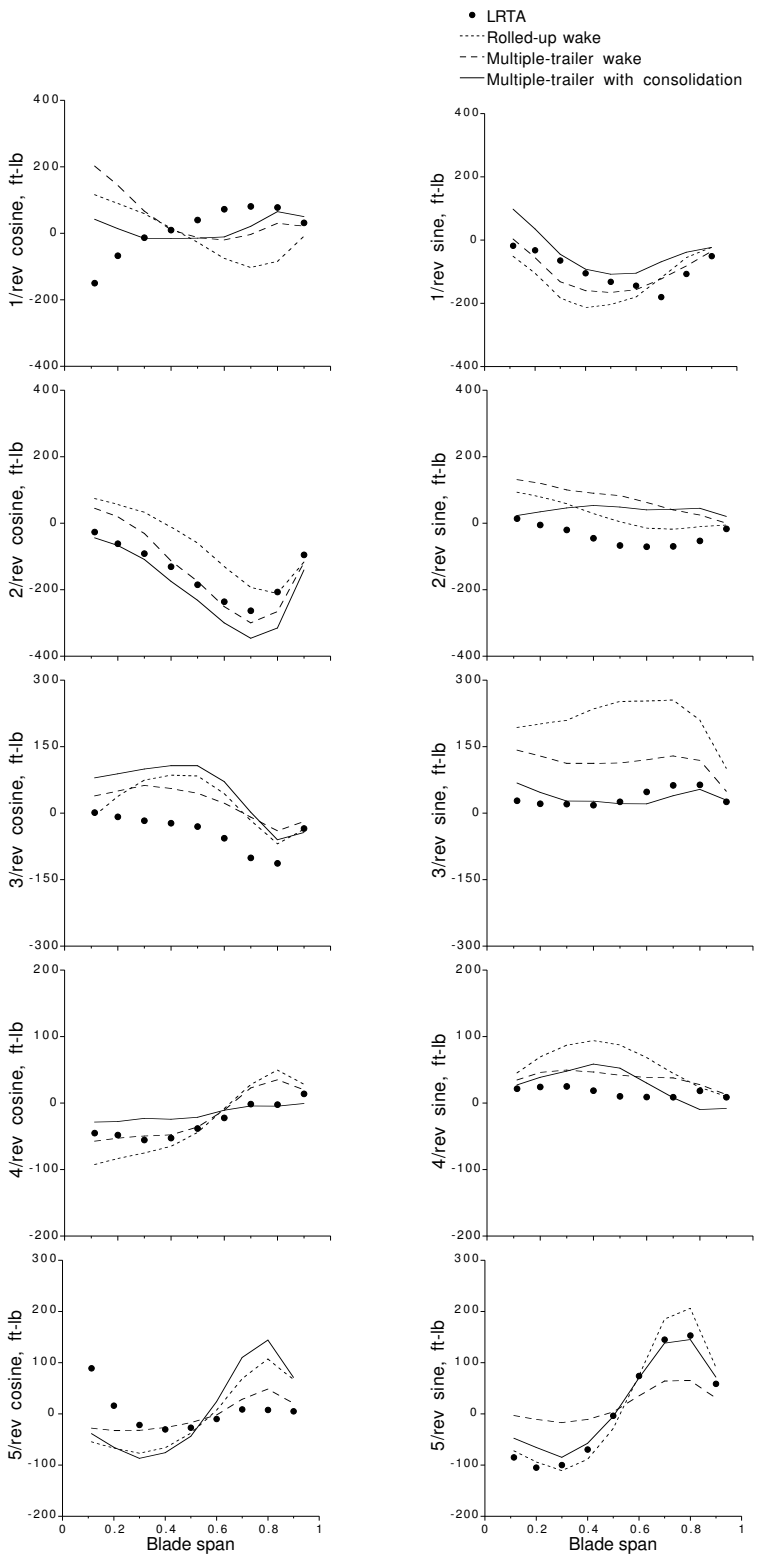

Fig. 27 Comparison of cosine and sine harmonics of flap bending moment with wind tunnel test data for $C_T/\sigma = 0.08$, $\mu = 0.10$, shaft pitch = -5.0 deg